HHS Public Access

Author manuscript

Mol Cell Neurosci. Author manuscript; available in PMC 2016 September 01.

Published in final edited form as:

Mol Cell Neurosci. 2015 September ; 68: 120–130. doi:10.1016/j.mcn.2015.04.005.

Dopamine transporter is enriched in filopodia and induces filopodia formation

John Caltagarone, **Shiqi Ma**, and **Alexander Sorkin**

Department of Cell Biology, University of Pittsburgh School of Medicine, Pittsburgh, PA 15261

Abstract

Dopamine transporter (DAT, *SLC6A3*) controls dopamine (DA) neurotransmission by mediating re-uptake of extracellular DA into DA neurons. DA uptake depends on the amount of DAT at the cell surface, and is therefore regulated by DAT subcellular distribution. Hence we used spinning disc confocal microscopy to demonstrate DAT localization in membrane protrusions that contained filamentous actin and myosin X (MyoX), a molecular motor located in filopodia tips, thus confirming that these protrusions are filopodia. DAT was enriched in filopodia. In contrast, R60A and W63A DAT mutants with disrupted outward-facing conformation were not accumulated in filopodia, suggesting that this conformation is necessary for DAT filopodia targeting. Three independent approaches of filopodia counting showed that DAT expression leads to an increase in the number of filopodia per cell, indicating that DAT can induce filopodia formation. Depletion of MyoX by RNA interference resulted in a significant loss of filopodia but did not completely eliminate filopodia, implying that DAT-enriched filopodia can be formed without MyoX. In cultured postnatal DA neurons MyoX was mainly localized to growth cones that displayed highly dynamic DAT-containing filopodia. We hypothesize that the concave shape of the DAT molecule functions as the targeting determinant for DAT accumulation in outward-curved membrane domains, and may also allow high local concentrations of DAT to induce an outward membrane bending. Such targeting and membrane remodeling capacities may be part of the mechanism responsible for DAT enrichment in the filopodia and its targeting to the axonal processes of DA neurons.

Keywords

dopamine transporter; filopodia; myosin X

*Corresponding author: Alexander Sorkin, Department of Cell Biology, University of Pittsburgh School of Medicine, S368 Biomedical Science Tower South, 3500 Terrace Street, Pittsburgh, PA 15261, Phone: 412-6243116, FAX: 412-648-8330, sorkin@pitt.edu.

The authors have no conflict of interest to declare.

INTRODUCTION

Dopamine (DA) signaling in the central nervous system is involved in various aspects of locomotor activity, emotions, reward, and affect (Iversen and Iversen, 2007). Dysfunctions of the DA system are implicated in a spectrum of abnormalities, such as Parkinson's disease, schizophrenia, bipolar disorder, attention deficit hyperactivity disorder, and psychostimulant drug abuse (Hyman et al., 2006; Ueno, 2003). In mouse brain the somatodendritic compartments of DA neurons are located in the midbrain, in particular in the substantia nigra and ventral tagmental area. During development these neurons project axons mainly to striatum to form a highly elaborate axonal network. The amplitude and duration of the dopaminergic neurotransmission is controlled by the regulation of extracellular DA concentrations via reuptake by the plasma membrane DA transporter (DAT) (Gether et al., 2006; Schmitz et al., 2003). DAT is expressed exclusively in DA neurons with the highest concentration in striatal axons. The mechanisms responsible for targeting of DAT, that is synthesized in the somatodendritic compartments of DA neurons in the midbrain, to the axonal processes of these neurons in the striatum and maintaining high levels of DAT in axons are unknown.

DAT functions in the plasma membrane, and therefore, subcellular localization and trafficking of DAT are important for its activity. For instance, regulation of DAT surface levels by endocytosis has been proposed (Melikian, 2004). In addition, DAT activity is regulated by its sub-compartmentalization in specialized domains of the plasma membrane (Adkins et al., 2007; Foster et al., 2008; Hong and Amara, 2010). We have previously demonstrated DAT localization in filopodia-like membrane protrusions in non-neuronal cells and primary mesencephalic cultures of DA neurons (Rao et al., 2012; Sorkina et al., 2009). Interestingly, DAT was less mobile in these membrane protrusions than in other regions of the plasma membrane (Rao et al., 2012; Sorkina et al., 2009). We then hypothesized that targeting to membrane protrusions serves to retain functional DAT at the cell surface.

In the present study we addressed three main questions. First, are DAT-containing structures actually the filopodia or other types of membrane protrusive structures? Filopodia are broadly defined as thin (0.1–0.3 μm), finger-like structures that are filled with tight parallel bundles of filamentous (F)-actin (Mattila and Lappalainen, 2008). In neurons filopodia have important roles in axonal outgrowth, branching, cell migration, dendritic spine formation and interneuron communication (Gallo, 2011; Gallo, 2013). Second, is DAT enriched in the filopodia-like protrusions? In other words, is concentration of DAT higher in these protrusions than in other areas of the membrane? Third, if DAT is enriched in filopodia-like protrusions, is it targeted to pre-existing protrusions or capable to induce *de novo* formation of membrane protrusions and maintain these structures? To address these questions, the localization of DAT and its mutants was analyzed using fluorescence microscopy imaging in comparison with subcellular distribution of other membrane proteins, F-actin and resident filopodia proteins.

MATERIALS AND METHODS

Reagents

Antibodies were purchased from the following sources: mouse monoclonal antibody to hemagglutinin epitope HA11 (16B12, cat# MMS-101P) and HA11 conjugated with Alexa488 (HA11-A488, cat# A488-101L) were from Covance (Berkley, CA); rabbit polyclonal myosin X (MyoX) antibody (working dilution 1:100–500 and 1:1000 in immunofluorescence and western blotting experiments, respectively) from Sigma Aldrich (St. Louis, MO) (cat# HPA024223); rabbit polyclonal antibody to α-actinin from Cell Signaling Technology (cat#3134S; working dilution 1:1000). Mouse monoclonal antibody to epidermal growth factor receptor (EGFR) Mab528 was from American Type Cell Culture Collections, Inc. (Manassas, VA) (cat#HB-8509). Mouse monoclonal antibody to vasodilator-stimulated phosphoprotein (VASP) (BD Biosciences, cat#610447, working dilution 1:100) was a kind gift from Dr. Partha Roy (McGowan Institute for Regenerative Medicine, Pittsburgh). Donkey anti-mouse, anti-rat and anti-rabbit antibodies conjugated with Alexa488, Cy5 or Cy3 (working dilution 1:250–500) were from Jackson Immuno Research (West Grove, PA); IRDye-800 and IRDye-680-conjugated goat anti-rabbit antibodies were purchased from LI-COR Biosciences (Lincoln, NE) (working dilution 1:10,000). Protein G-Sepharose was purchased from Invitrogen (Carlsbad, CA). Cell Mask Deep Red Plasma Membrane Stain (CellMask, cat#C10046) and phalloidin-Alexa680 (cat#A22286) (working dilution 1:500) were from Invitrogen. Paraformaldehyde was from Electron Microscopy Sciences (Hatfield, PA). Tissue culture reagents were purchased from Invitrogen. Triton X-100, protease Inhibitors and most other reagents were purchased from Sigma Aldrich.

DNA constructs

Wild-type and mutants (W63A and R60A) of yellow fluorescent protein (YFP) and hemaglutinin epitope (HA) tagged human DAT (YFP-HA-DAT) were described previously (Sorkina et al., 2009). To generate RFP (red fluorescent protein)-HA-DAT, HA-DAT sequence from the YFP-HA-DAT construct was inserted into the tagRFP-C1 vector (provided by Dr. V. Verkhusha, Albert Einstein College of Medicine) using *Kpn*I restriction site at the 5′-end and a *Sma*I site at the 3′-end. Lifeact-RFP described in (Berepiki et al., 2010) was provided by Dr. Lichius (University of Edinburgh, Edinburgh, UK). EGFR mutant construct lacking the entire cytoplasmic domain (EGFR-ΔC) was described previously (Miranda et al., 2004). GFP (green fluorescent protein)-MyoX described in (Berg and Cheney, 2002) was provided by Dr. R. E. Cheney (University of North Carolina). RFP-CAAX construct, which consisted of monomeric RFP with the membrane-targeting H-Ras sequence KLNPPDESGPGCMSCKCVLS attached in frame to the C-terminus of RFP and cloned into pCS2+ vector (Wallingford et al., 2000), was provided by P. K. Umasanker (University of Pittsburgh).

Cell culture, transfections and RNA interference

Parental and DAT-expressing porcine aortic endothelial (PAE) cells were grown in F12 medium with 10% fetal bovine serum (FBS). PAE cells constitutively expressing YFP-HA-DAT (PAE/YFP-HA-DAT) were described previously (Sorkina et al., 2009). PAE cells

constitutively expressing RFP-HA-DAT (PAE/RFP-HA-DAT) were generated by selection in the presence of G418 (400 μg/ml). HEK293T and HeLa cells were grown on DMEM with 10% FBS. All cell lines were regularly checked for mycoplasma using Lonza (Allendale, NJ) mycoplasma detection kit. For live imaging cells were grown on collagen-coated glass bottom 35 mm dishes (Mat-Tek, Ashland, MA) or Poly-D-Lysin (Sigma)-covered glass coverslips, and for immunofluorescence staining experiments the cells were grown on glass coverslips.

The cells were transfected with DNA plasmids using Lipofectamine (Invitrogen) or Effectine (Qiagen, Valencia, CA) kits following manufacturer's protocols.

ON-TARGET SMARTpool siRNA to MyoX (cat# J-007217-05) and non-targeting siRNA (cat# 1027310) were purchased from Thermo Fisher Scientific (Pittsburgh, PA) and Qiagen, respectively. siRNA transfections were performed with DharmaFECT® Transfection Reagent #1 from Thermo Fisher Scientific according to manufacturer's recommendations and as described previously (Sorkina et al., 2013). Typically, cells were assayed 72 hours after siRNA transfection. Efficiency of MyoX knock-down was determined in each experiment by immunofluorescence and Western blotting.

DA neuronal cultures

Primary mesencephalic postnatal cultures were prepared from HA-DAT knock-in mice as previously described (Ding et al., 2004; Rao et al., 2012). Experiments were performed on neurons at days in vitro (DIV) 6–10. Cultures were grown on glass coverslips pre-covered with Poly-D-Lysine and laminin. All animal studies were performed according to an approved IACUC protocol.

Fluorescence microscopy

For live-cell imaging, the cells grown on Mat-Tek dishes or glass coverslips were placed onto the stage of the spinning disk confocal imaging system based on a Zeiss Axio Observer Z1 inverted fluorescence microscope (with 63x Plan Apo PH NA 1.4), equipped with a computer-controlled Spherical Aberration Correction unit, Yokogawa CSU-X1, Vector photomanipulation module, Photometrics Evolve 16-bit EMCCD camera, HQ2 cooled CCD camera, environmental chamber and piezo stage controller and lasers (405, 445, 488, 515, 561, and 640 nm) (Intelligent Imaging Innovations, Inc., Denver, CO), all controlled by SlideBook software (Intelligent Imaging Innovation, Denver, CO). To obtain high resolution 3D images of the cells, a z-stack of 10–20 confocal images at 200–400 nm z-stepsize were acquired with 37°C, humidity and 5% CO_2 atmosphere maintained throughout the duration of the imaging. Image acquisition settings were identical during imaging of all experimental variants in each experiment.

For immunofluorescence staining, cells on coverslips were washed with ice-cold PBS (Invitrogen) and fixed with freshly prepared 4% paraformaldehyde for 15 min at room temperature. To detect surface EGFR (transient expression of EGFR-ΔC), the cells were incubated with EGFR antibody Mab528 and subsequently with the secondary anti-mouse antibody conjugated to Cy5. To detect MyoX and other intracellular proteins, fixed cells were permeabilized with 0.1–2 % Triton X-100 for 3 min and incubated with appropriate

primary and secondary antibodies in PBS containing either 0.5% BSA or 0.05% Tween-20. Each antibody incubation was followed by three 2-min wash in the same buffers. Both primary and secondary antibody solutions were pre-cleared by centrifugation at 100,000 × g for 20 min. Coverslips were mounted in ProLong Gold (Invitrogen).

Image analysis

The ratio of RFP and YFP fluorescence was quantitated by generating a maximum projection image from a 3D image. One mask was generated to manually select peripheral filopodia, and another mask to select multiple regions in other parts of cell including lamellopodia, ruffles and “flat” plasma membrane. RFP and YFP fluorescence intensities were calculated from background-subtracted images using the statistics module of SlideBook.

The number of filopodia was determined by utilizing a maximum projection image from a 3D image. A selection mask was generated to manually select the entire “cell body”. Filopodia longer than 2 μm were counted in different experimental variants by two researchers in a blind fashion. The perimeter of the cell body was calculated using the statistics module of the SlideBook. The filopodia density was expressed as number of filopodia per 100 μm of cell perimeter. The examples of images and masks are presented in Fig. 4. The lengths of filopodia were also measured using SlideBook.

Western blotting

Cells were lysed, lysates were electrophoresed, and western blotting was performed as described previously (Sorkina et al., 2013).

Statistical analysis

Statistical significance (P value) was calculated using unpaired Student’s t tests (GraphPad and Excel). Data normality of all data sets with the exception of the data used to measure the effects of MyoX siRNA was confirmed using the D’Agostino-Pearson test (GraphPad).

RESULTS

DAT-containing membrane protrusions are filopodia

Previous studies demonstrated localization of DAT in filopodia-like membrane protrusions in non-neuronal cells and cultured post-natal dopaminergic neurons (Rao et al., 2012; Sorkina et al., 2009). To test whether these protrusions containing DAT are “classical” filopodia, DAT localization was compared with that of filamentous (F)-actin and a marker of filopodia, unconventional myosin, MyoX (also known as myosin 10) (Berg and Cheney, 2002). PAE cells were used as the main experimental model because DAT efficiently exits endoplasmic reticulum and is delivered to the plasma membrane when transiently or stably expressed in these cells. Staining of PAE/RFP-HA-DAT with Alexa680 labeled phalloidin revealed the presence of F-actin in RFP-HA-DAT containing membrane extensions (Fig. 1A). Remarkably, MyoX immunofluorescence was concentrated on the tips of many DAT-labeled membrane protrusions that extended from the cell edge, dorsal membrane and large

ruffle-like structures (Fig. 1A). Substantial intracellular staining of MyoX was also observed, likely due to non-specific antibody binding.

Three-dimensional (3D) imaging of living cells co-expressing GFP-MyoX and RFP-HA-DAT demonstrated the localization of GFP-MyoX on the tips of RFP-HA-DAT-containing finger-like membrane protrusions (Fig. 1B). Similar co-localization of MyoX and DAT in membrane protrusions was observed in COS1 and HEK293 cells (Supplemental Figure S1A). Furthermore, VASP, a protein that is thought to regulate actin filament elongation in the filopodia (Schirenbeck et al., 2006), was detected in the shafts and tips of some DAT-containing protrusions (Fig. S1B). Time-lapse 3D imaging demonstrated that peripheral and dorsal filopodia were highly mobile with rapid lateral, protruding and retracting motions which distinguishes them from retraction fibers (Fig. 2A, supplemental video S1). Altogether these data strongly argue that DAT-containing membrane protrusions are indeed filopodia.

DAT is enriched in filopodia

To test whether DAT is enriched in filopodia, PAE cells stably expressing YFP (yellow fluorescent protein)-HA-DAT (PAE/YFP-HA-DAT) were stained with the membrane probe CellMask or transfected with the membrane-targeted RFP (RFP-CAAX). These general membrane markers weakly labeled and did not penetrate into distal parts of DAT-containing filopodia, suggesting an enrichment of DAT in these structures relative to filopodia-free plasma membrane areas (Supplemental Figure S2). However, both CellMask and RFP-CAAX were also present in internal membranes, which complicated the quantitation of relative concentrations in the plasma membrane. In order to compare the distribution of DAT with an unrelated integral membrane protein, a mutant of EGFR, in which the entire cytosolic domain was truncated (EGFR-ΔC), was co-expressed with YFP-HA-DAT. EGFR-ΔC predominantly localizes to the plasma membrane, and in our staining procedure (see Methods), only surface exposed EGFR-ΔC was detected. As shown in Fig. 2B, YFP-HA-DAT and EGFR-ΔC were located in the same filopodia. However, the ratio of YFP fluorescence to EGFR-ΔC immunofluorescence intensities was significantly higher in filopodia than in other parts of the cell (Fig. 2C). This result suggests that YFP-HA-DAT is concentrated in filopodia as compared with a more evenly-distributed EGFR-ΔC. The data of Figs. 2B and C, therefore, indicate that DAT is enriched in filopodia.

Conformation-defective DAT mutants do not concentrate in filopodia

Demonstration of DAT accumulation in filopodia prompted the investigation of the mechanism of such targeting. Various mechanisms may contribute to protein targeting to specific membrane domains, but sorting mechanisms based on the affinity of certain protein conformations to specific membrane shapes are particularly compelling, because some regions of the membranes, such as for example filopodia, are highly curved (Aimon et al., 2014). The proposed model of DAT function suggests conformational transition during substrate movement through the transporter from an outward-facing conformation capable of binding to the extracellular substrate and sodium ions, through the substrate-occluded state, and to an inward-facing conformation leading to the release of the substrate into cytoplasm (Yamashita et al., 2005). We have previously observed that DAT mutants with

disrupted outward-facing conformation appear to not concentrate in membrane protrusions, although this could be due to different expression levels of wild-type and mutant DAT in stable cell clones (Sorkina et al., 2009). To directly compare the localization of wild-type and mutant DATs, RFP-HA-DAT was transiently co-expressed with W63A or R60A mutants of YFP-HA-DAT in PAE cells. Both DATs were highly co-localized in all areas of the cell including filopodia (Figs. 3A and C). Interestingly, the ratio of RFP to YFP fluorescence intensities (RFP/YFP) in filopodia was substantially higher than in other regions of the cell (Fig. 3B and D). In fact, distal parts of many RFP-HA-DAT containing filopodia did not contain detectable amounts of W63A or R60A mutants regardless of the expression levels of wild-type and mutant DATs. Overall the subcellular distribution of these DAT mutants was similar to that observed for EGFR-ΔC. The extent of the differential distribution of wild-type versus mutant DAT observed in co-expression experiments was probably underestimated because of wild-type/mutant DAT hetero-oligomerization (Sorkina et al., 2003; Torres et al., 2003). Altogether, these results suggest that an outward-facing conformation is necessary for DAT accumulation in filopodia.

Expression of DAT induces filopodia formation

Analysis of images similar to those presented in Fig. 3 revealed that cells expressing wild-type DAT had on average 34% more filopodia longer than 10 μm than the cells expressing DAT mutants. Further, visual inspection of hundreds of images suggested that cells with high expression levels of DAT tend to have the highest density of DAT-containing filopodia. Therefore, we tested whether wild-type DAT can promote filopodia formation by counting filopodia in cells expressing and not expressing DAT. Several approaches of filopodia labeling and counting were used. To perform this analysis in living cells, PAE cells were transfected with Lifeact-RFP to label F-actin, and with YFP-HA-DAT or YFP. Live-cell 3D imaging of Lifeact-RFP revealed large stress fibers in cell body and smaller filaments that were detected in filopodia containing YFP-HA-DAT, although Lifeact-RFP did not penetrate into distal parts of these filopodia (Fig. 4A). Analysis of Lifeact-RFP images revealed a statistically significant increase in the peripheral filopodia membrane density in cells expressing YFP-HA-DAT over control cells as measured by the number of filopodia per unit of the cell perimeter (Fig. 4B–D). In the second approach, numbers of MyoX positive filopodia tips were counted in fixed PAE/YFP-HA-DAT and parental PAE cells. This analysis also demonstrated a higher number of filopodia in cells expressing YFP-HA-DAT (Fig. 4D). Finally, PAE cells were co-transfected with EGFR-ΔC and YFP-HA-DAT or YFP. In these experiments, an increased density of EGFR-ΔC labeled filopodia was observed in YFP-HA-DAT expressing cells as compared to control cells (Fig. 4D). In all three approaches the number of peripheral filopodia per length of the perimeter of the cell was calculated. Dorsal filopodia were difficult to count, especially in fixed cells, because of their overlap with the strong fluorescence of actin, MyoX and EGFR-ΔC staining throughout the perinuclear area of the cell. However, it is likely that the numbers of DAT-enriched filopodia were underestimated because Lifeact-RFP and EGFR-ΔC did not penetrate to the entire length of DAT-enriched filopodia, and may therefore, be undetectable in short filopodia. Likewise, not all DAT-enriched filopodia contained MyoX at the tips (Fig. 1). Nevertheless, all three approaches to detect and count filopodia indicated that DAT can induce and/or maintain filopodia in both transiently and stably DAT-expressing cells.

Knockdown of MyoX reduces filopodia density

MyoX is involved in filopodia formation (Bohil et al., 2006) and is highly co-localized with DAT-enriched filopodia. However, some DAT enriched filopodia did not contain detectable MyoX, although the morphology and dynamics of these protrusions at the light microscopic level was indistinguishable from that of the protrusions with MyoX at the tips (Fig. 1). To directly test whether MyoX is required for formation and/or maintenance of DAT-enriched filopodia, the effect of MyoX siRNA knock-down on filopodia was examined in PAE/YFP-HA-DAT and PAE/RFP-HA-DAT cells. Depletion of MyoX is evident by virtually complete disappearance of MyoX immunoreactivity from the tips of filopodia (Fig. 5A), although a significant amount of immunofluorescence staining remained in the perinuclear areas of the cells. Since “headless” splicing form of MyoX (Lin et al., 2013) was not detected in PAE cells, the intracellular immunofluorescence in siRNA transfected cells is likely due to non-specific antibody binding. Analysis of multiple 3D images of YFP-HA-DAT and RFP-HA-DAT expressing cells showed that many MyoX-depleted cells were devoted of both peripheral and dorsal filopodia containing DAT (Fig. 5A and B). MyoX depletion also resulted in accumulation of DAT in lamellopodia-like structures near cell edges in many cells (Fig. 5A and B). It should be emphasized that a substantial number of DAT-enriched filopodia were seen, in particular, in contacting MyoX-depleted cells, despite not detecting MyoX in these filopodia tips. The morphology and dynamics of these filopodia were similar to that in MyoX-expressing cells. These data suggest that MyoX is involved in the formation and maintenance of DAT-enriched/induced filopodia but is not essential for these processes.

DAT containing filopodia and localization of MyoX in DA neurons

MyoX and filopodia are important for axonal pathfinding, neurite outgrowth, spine formation and related processes (Ju et al., 2014; Sousa et al., 2006; Zhu et al., 2007). We have previously demonstrated the localization of DAT in dynamic axonal filopodia in primary cultures of post-natal midbrain DA neurons (Rao et al., 2012). Co-staining of DAT with MyoX in post-natal DA neurons obtained from HA-DAT knock-in mice (Rao et al., 2012) revealed the predominant location of MyoX in growth cones (Fig. 6A–B). Live-cell imaging of DA neurons incubated with HA11 antibody conjugated with Alexa488 demonstrated high motility of filopodia containing HA-DAT in growth cones (Fig. 6C–D, supplemental videos S2 and S3). On the other hand, highly dynamic filopodia extending from axonal shafts and varicosities previously observed by live-cell microscopy [(Rao et al., 2012) and data not shown] were difficult to detect in fixed DA neurons by immunofluorescence staining, presumably, because of the fragile nature of these structures and high non-specific staining backgrounds. MyoX was not detected in the tips of growth cone filopodia by immunofluorescence staining. It should be noted that we have not identified a MyoX antibody that efficiently detects mouse MyoX by immunofluorescence, which may have prevented the detection of tip-located MyoX in neurons. In summary, studies in cultured DA neurons suggest that DAT-containing growth cone filopodia may form and function independently of the MyoX function in the filopodia tip complex.

DISCUSSION

In this study we used fluorescence microscopy imaging of living and fixed cells to demonstrate that finger-like membrane protrusions containing DAT are the “conventional” filopodia, and to analyze the mechanisms of DAT targeting to these filopodia. The filopodia nature of DAT containing protrusions was evident from the high extent of DAT co-localization with the actin-associated motor MyoX in various types of cells heterologously expressing DAT (Figs. 1, S1 and 5). MyoX was located in the tips of the peripheral filopodia that extend from cell edges and dorsal filopodia that emanate from the dorsal membrane of the substrate-attached cells. The highest concentration of the filopodia containing DAT and MyoX was typically observed in the area of cell contacts. This is consistent with the recent finding that MyoX is involved in the formation of intercellular tunneling nanotubes forming from directed protrusion of dorsal filopodia (Gousset et al., 2013).

The demonstration that DAT is enriched in filopodia in comparison to the general membrane probes and a model integral membrane protein (Fig. 2) is important as it suggests that filopodia provide a targeting platform for DAT. Moreover, DAT mutants with disrupted outward-facing conformation were not enriched in filopodia when co-expressed with wild-type DAT in the same cell (Fig. 3). This finding implies that an outward-facing conformation of DAT is necessary for the maximal accumulation of DAT in filopodia.

The increased numbers of filopodia in cells transiently or stably expressing DAT is a surprising finding (Fig. 4). This finding suggests that DAT may induce formation and/or maintain filopodia. The mechanisms of filopodia formation, maintenance and motility are not fully understood. Membrane bending by an I-BAR-domain-containing IRSp53 protein together with actin polymerization regulated by cdc42 are thought to be involved in the initial stages of filopodia formation, although cdc42 is not necessary for all types of filopodia (Mattila and Lappalainen, 2008; Sigal et al., 2007; Yang et al., 2009). VASP was proposed to regulate actin polymerization at the barbed ends of actin filaments to allow the extension of the filopodium, and it was proposed that MyoX is responsible for the delivery of VASP to the filopodium tip complex (Lin et al., 2013; Tokuo and Ikebe, 2004). However, formation of DAT-enriched filopodia did not absolutely require VASP and MyoX. Firstly, VASP was detected only in a small number of DAT-enriched filopodia (Fig. S1B), and a population of DAT-containing filopodia also did not contain MyoX (Figs. 1, S1, 5). Secondly, knockdown of MyoX reduced the number of DAT-enriched filopodia but did not completely eliminate them (Fig. 5). This is in agreement with the partial effect of MyoX knockdown on dorsal filopodia in HeLa cells (Bohil et al., 2006). Furthermore, although another proposed function of MyoX is to transport integrins to the tip of filopodia, thus leading to filopodia substrate attachment (Zhang et al., 2004), most peripheral DAT-enriched filopodia displayed rapid movements and were not attached to the substrate (Fig. 2A). Therefore, we hypothesized that filopodia can be induced by the local concentration of DAT, and that these filopodia can be, at least temporarily, sustained without VASP and MyoX.

The morphology and other characteristics of DAT-enriched/induced filopodia are reminiscent to that of the filopodia induced by overexpression of lipid-phosphatase-related

protein 1 (Sigal et al., 2007). Further, expression of vβ2 auxiliary subunit of voltage-gated sodium channel appears to also induce filopodia-like membrane protrusions (Maschietto et al., 2013). We propose that the ability to accumulate in highly curved membrane regions, such as in the filopodia membrane, and induce filopodia formation may be a property of a wide range of transmembrane proteins. Recently, an enrichment in curved membranes and induction of membrane remodeling by purified integral membrane proteins was demonstrated in *in vitro* experiments in giant unilamellar vesicles (Aimon et al., 2014).

In summary, we propose the following hypothetic model. Because functional DAT molecule is thought to have a convex shape (Penmatsa et al., 2013; Yamashita et al., 2005), DAT may concentrate in outward-curved membranes. Moreover, high local concentrations of DAT may promote membrane deformation and outward bending, thus generating membrane protrusions like filopodia that are then stabilized and regulated by actin filaments and associated machinery including MyoX. Disruption of the intramolecular interactions necessary for the outward-open conformation of DAT by W63A and R60A mutations are predicted to minimize the probability of the convex-shaped conformation of DAT (Penmatsa et al., 2013; Yamashita et al., 2005), which would at least partially abolish DAT targeting to filopodia and its filopodia-inducing capacity.

Enrichment of DAT in the filopodia and other membrane regions with high outward curvature, and the ability to induce filopodia may be important for normal development and organization of DA neurons. Developmentally increasing expression of DAT may augment filopodia formation, and therefore, facilitate synaptogenesis processes in the striatum. Growth cone filopodia enriched in DAT are highly dynamic (Fig. 6). Although these filopodia did not contain detectable MyoX at the tips, MyoX was concentrated in growth cones (Fig. 6), similarly to what was observed in spinal motorneurons (Plantman et al., 2013). It is possible that the function of MyoX in growth cones is different from its function as an organizer of the filopodia tip complex. It is also possible that a headless form of MyoX (Lin et al., 2013) is predominantly expressed in postnatal DA neurons. Finally, limitations in the specificity of MyoX antibodies (all commercially available antibodies were tested) may have prevented the detection of MyoX at the filopodia tips in DA neurons. Furthermore, filopodia-formation activity of DAT may not be essential during development as a number of guidance receptors and ion transport proteins are present in the growth cone filopodia. On the other hand, the capacity of DAT to concentrate in highly-curved plasma membrane compartments, such as filopodia, may be part of the mechanism by which DAT accumulates in striatal axonal processes. These axons have the diameter comparable to that of DAT-enriched filopodia, and therefore may be rich in curved membrane regions. Such targeting mechanism would explain high concentration of DAT throughout thin axonal shafts and in synaptic areas of DA neurons while relatively low DAT abundance in the somatic compartment of these neurons.

Supplementary Material

Refer to Web version on PubMed Central for supplementary material.

Acknowledgments

We thank Drs. Cheney, Lichius, Roy, Umasanker and Verkhusha for generous gifts of the reagents. This work was supported by NIH/NIDA grants DA014204 (J. C, S. M. and A.S.) and T32DA031111 (J. C.).

Abbreviations

F-actin	filamentous actin
DA	dopamine
DAT	dopamine transporter
EGFR	epidermal growth factor receptor
HA	hemagglutinin epitope
MyoX	myosin X or myosin 10
VASP	vasodilator-stimulated phosphoprotein
GFP	RFP and YFP, green, red and yellow fluorescent proteins, respectively

LITERATURE CITED

Adkins EM, Samuvel DJ, Fog JU, Eriksen J, Jayanthi LD, Vaegter CB, Ramamoorthy S, Gether U. Membrane mobility and microdomain association of the dopamine transporter studied with fluorescence correlation spectroscopy and fluorescence recovery after photobleaching. Biochemistry. 2007; 46:10484–97. [PubMed: 17711354]

Aimon S, Callan-Jones A, Berthaud A, Pinot M, Toombes GE, Bassereau P. Membrane shape modulates transmembrane protein distribution. Developmental cell. 2014; 28:212–8. [PubMed: 24480645]

Berepiki A, Lichius A, Shoji JY, Tilsner J, Read ND. F-actin dynamics in Neurospora crassa. Eukaryotic cell. 2010; 9:547–57. [PubMed: 20139238]

Berg JS, Cheney RE. Myosin-X is an unconventional myosin that undergoes intrafilopodial motility. Nature cell biology. 2002; 4:246–50. [PubMed: 11854753]

Bohil AB, Robertson BW, Cheney RE. Myosin-X is a molecular motor that functions in filopodia formation. Proceedings of the National Academy of Sciences of the United States of America. 2006; 103:12411–6. [PubMed: 16894163]

Ding YM, Jaumotte JD, Signore AP, Zigmond MJ. Effects of 6-hydroxydopamine on primary cultures of substantia nigra: specific damage to dopamine neurons and the impact of glial cell line-derived neurotrophic factor. Journal of Neurochemistry. 2004; 89:776–87. [PubMed: 15086533]

Foster JD, Adkins SD, Lever JR, Vaughan RA. Phorbol ester induced trafficking-independent regulation and enhanced phosphorylation of the dopamine transporter associated with membrane rafts and cholesterol. J Neurochem. 2008; 105:1683–99. [PubMed: 18248623]

Gallo G. The cytoskeletal and signaling mechanisms of axon collateral branching. Developmental neurobiology. 2011; 71:201–20. [PubMed: 21308993]

Gallo G. Mechanisms underlying the initiation and dynamics of neuronal filopodia: from neurite formation to synaptogenesis. Int Rev Cell Mol Biol. 2013; 301:95–156. [PubMed: 23317818]

Gether U, Andersen PH, Larsson OM, Schousboe A. Neurotransmitter transporters: molecular function of important drug targets. Trends in Pharmacological Sciences. 2006; 27:375–383. [PubMed: 16762425]

Gousset K, Marzo L, Commere PH, Zurzolo C. Myo10 is a key regulator of TNT formation in neuronal cells. Journal of Cell Science. 2013; 126:4424–35. [PubMed: 23886947]

Hong WC, Amara SG. Membrane cholesterol modulates the outward facing conformation of the dopamine transporter and alters cocaine binding. The Journal of biological chemistry. 2010; 285:32616–26. [PubMed: 20688912]

Hyman SE, Malenka RC, Nestler EJ. Neural mechanisms of addiction: the role of reward-related learning and memory. Annu Rev Neurosci. 2006; 29:565–98. [PubMed: 16776597]

Iversen SD, Iversen LL. Dopamine: 50 years in perspective. Trends Neurosci. 2007; 30:188–93. [PubMed: 17368565]

Ju XD, Guo Y, Wang NN, Huang Y, Lai MM, Zhai YH, Guo YG, Zhang JH, Cao RJ, Yu HL, et al. Both Myosin-10 isoforms are required for radial neuronal migration in the developing cerebral cortex. Cerebral cortex. 2014; 24:1259–68. [PubMed: 23300110]

Lin WH, Hurley JT, Raines AN, Cheney RE, Webb DJ. Myosin X and its motorless isoform differentially modulate dendritic spine development by regulating trafficking and retention of vasodilator-stimulated phosphoprotein. Journal of Cell Science. 2013; 126:4756–68. [PubMed: 23943878]

Maschietto M, Girardi S, Dal Maschio M, Scorzeto M, Vassanelli S. Sodium channel beta2 subunit promotes filopodia-like processes and expansion of the dendritic tree in developing rat hippocampal neurons. Frontiers in cellular neuroscience. 2013; 7:2. [PubMed: 23355803]

Mattila PK, Lappalainen P. Filopodia: molecular architecture and cellular functions. Nat Rev Mol Cell Biol. 2008; 9:446–54. [PubMed: 18464790]

Melikian HE. Neurotransmitter transporter trafficking: endocytosis, recycling, and regulation. Pharmacol Ther. 2004; 104:17–27. [PubMed: 15500906]

Miranda M, Sorkina T, Grammatopoulos TN, Zawada WM, Sorkin A. Multiple molecular determinants in the carboxyl terminus regulate dopamine transporter export from endoplasmic reticulum. J Biol Chem. 2004; 279:30760–70. [PubMed: 15128747]

Penmatsa A, Wang KH, Gouaux E. X-ray structure of dopamine transporter elucidates antidepressant mechanism. Nature. 2013; 503:85–90. [PubMed: 24037379]

Plantman S, Zelano J, Novikova LN, Novikov LN, Cullheim S. Neuronal myosin-X is upregulated after peripheral nerve injury and mediates laminin-induced growth of neurites. Molecular and cellular neurosciences. 2013; 56:96–101. [PubMed: 23603155]

Rao A, Richards TL, Simmons D, Zahniser NR, Sorkin A. Epitope-tagged dopamine transporter knock-in mice reveal rapid endocytic trafficking and filopodia targeting of the transporter in dopaminergic axons. FASEB journal: official publication of the Federation of American Societies for Experimental Biology. 2012; 26:1921–33. [PubMed: 22267337]

Schirenbeck A, Arasada R, Bretschneider T, Stradal TE, Schleicher M, Faix J. The bundling activity of vasodilator-stimulated phosphoprotein is required for filopodium formation. Proceedings of the National Academy of Sciences of the United States of America. 2006; 103:7694–9. [PubMed: 16675552]

Schmitz Y, Benoit-Marand M, Gonon F, Sulzer D. Presynaptic regulation of dopaminergic neurotransmission. J Neurochem. 2003; 87:273–289. [PubMed: 14511105]

Sigal YJ, Quintero OA, Cheney RE, Morris AJ. Cdc42 and ARP2/3-independent regulation of filopodia by an integral membrane lipid-phosphatase-related protein. J Cell Sci. 2007; 120:340–52. [PubMed: 17200142]

Sorkina T, Caltagarone J, Sorkin A. Flotillins regulate membrane mobility of the dopamine transporter but are not required for its protein kinase C dependent endocytosis. Traffic. 2013; 14:709–24. [PubMed: 23418867]

Sorkina T, Doolen S, Galperin E, Zahniser NR, Sorkin A. Oligomerization of Dopamine Transporters Visualized in Living Cells by Fluorescence Resonance Energy Transfer Microscopy. J Biol Chem. 2003; 278:28274–28283. [PubMed: 12746456]

Sorkina T, Richards TL, Rao A, Zahniser NR, Sorkin A. Negative regulation of dopamine transporter endocytosis by membrane-proximal N-terminal residues. J Neurosci. 2009; 29:1361–74. [PubMed: 19193883]

Sousa AD, Berg JS, Robertson BW, Meeker RB, Cheney RE. Myo10 in brain: developmental regulation, identification of a headless isoform and dynamics in neurons. J Cell Sci. 2006; 119:184–94. [PubMed: 16371656]

Tokuo H, Ikebe M. Myosin X transports Mena/VASP to the tip of filopodia. Biochemical and biophysical research communications. 2004; 319:214–20. [PubMed: 15158464]

Torres GE, Carneiro A, Seamans K, Fiorentini C, Sweeney A, Yao WD, Caron MG. Oligomerization and trafficking of the human dopamine transporter. Mutational analysis identifies critical domains important for the functional expression of the transporter. J Biol Chem. 2003; 278:2731–9. [PubMed: 12429746]

Ueno S. Genetic polymorphisms of serotonin and dopamine transporters in mental disorders. Journal of Medical Investigation. 2003; 50:25–31. [PubMed: 12630565]

Wallingford JB, Rowning BA, Vogeli KM, Rothbacher U, Fraser SE, Harland RM. Dishevelled controls cell polarity during Xenopus gastrulation. Nature. 2000; 405:81–5. [PubMed: 10811222]

Yamashita A, Singh SK, Kawate T, Jin Y, Gouaux E. Crystal structure of a bacterial homologue of Na(+)/Cl(−)-dependent neurotransmitter transporters. Nature. 2005; 437

Yang C, Hoelzle M, Disanza A, Scita G, Svitkina T. Coordination of membrane and actin cytoskeleton dynamics during filopodia protrusion. PLoS One. 2009; 4:e5678. [PubMed: 19479071]

Zhang H, Berg JS, Li Z, Wang Y, Lang P, Sousa AD, Bhaskar A, Cheney RE, Stromblad S. Myosin-X provides a motor-based link between integrins and the cytoskeleton. Nature cell biology. 2004; 6:523–31. [PubMed: 15156152]

Zhu XJ, Wang CZ, Dai PG, Xie Y, Song NN, Liu Y, Du QS, Mei L, Ding YQ, Xiong WC. Myosin X regulates netrin receptors and functions in axonal path-finding. Nature cell biology. 2007; 9:184–92. [PubMed: 17237772]

Highlights

- DAT is accumulated in filopodia containing myosin X
- DAT mutants with disrupted outward-facing conformation are not enriched in filopodia
- DAT induces filopodia formation.
- We proposed that a concave shape of DAT mediates its accumulation in curved membranes

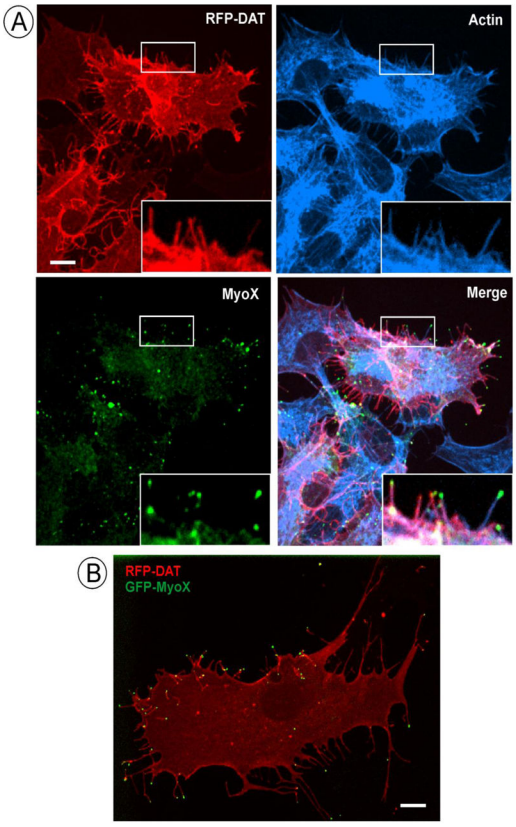

Figure 1. Membrane projection containing DAT are filopodia

(A) PAE/RFP-HA-DAT cells were fixed, stained with phalloidin-Alexa680, permeabilized and immunostained with rabbit polyclonal MyoX antibodies followed by secondary antibody conjugated to Alexa488. 3D images were acquired through 488 (green, MyoX), 561 (red, DAT-RFP) and 640 (cyan, actin) channels. Maximal projection of the z-stack is presented. Insets show high magnification of the region marked by white rectangles.

(**B**) GFP-MyoX was transiently expressed in PAE/RFP-HA-DAT cells, and 3D live-cell imaging was performed through 488 (green, GFP) and 561 (red, RFP) channels as described in “Methods”. A single x–y confocal image of merged GFP and RFP fluorescence is presented.

Scale bars, 10 μm.

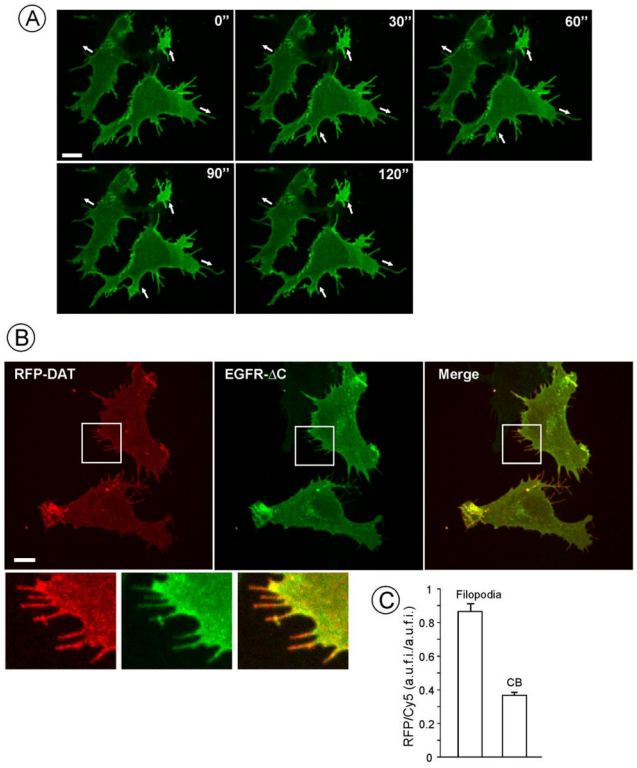

Figure 2. DAT is enriched in filopodia

(A) 4-D (3D and time-lapse) live-cell imaging of PAE/YFP-HA-DAT cells was performed at 37°C. Maximal projection images of the z-stack are presented. Individual time frames are shown. Times are in seconds. See Supplemental video S1. Arrows indicate protruding and retracting movements of membrane extensions. Scale bar, 10 μm.

(B) RFP-HA-DAT and EGFR-ΔC were transiently expressed in PAE cells, cells were fixed and stained with Ab528 (1 ng/mL) and Cy5-conjugated secondary antibody. 3D images were acquired through 561 and 640 filter channels. Maximal projection image is presented. Insets show high magnification of the region marked by the white rectangle to demonstrate enrichment of RFP-HA-DAT in distal filopodia regions as compared to EGFR-ΔC. Scale bar, 10 μm.

(**C**) Quantification of RFP/Cy5 fluorescence ratios in filopodia and other parts of the cells ("cell body", ***CB***) in images presented in ***A***. Graph bars represent mean values (+S.E.M.) of the RFP/YFP ratios from 30 filopodia or regions of interest (ROI) within CB. *A.u.f.i.*, arbitrary units of fluorescence intensity.

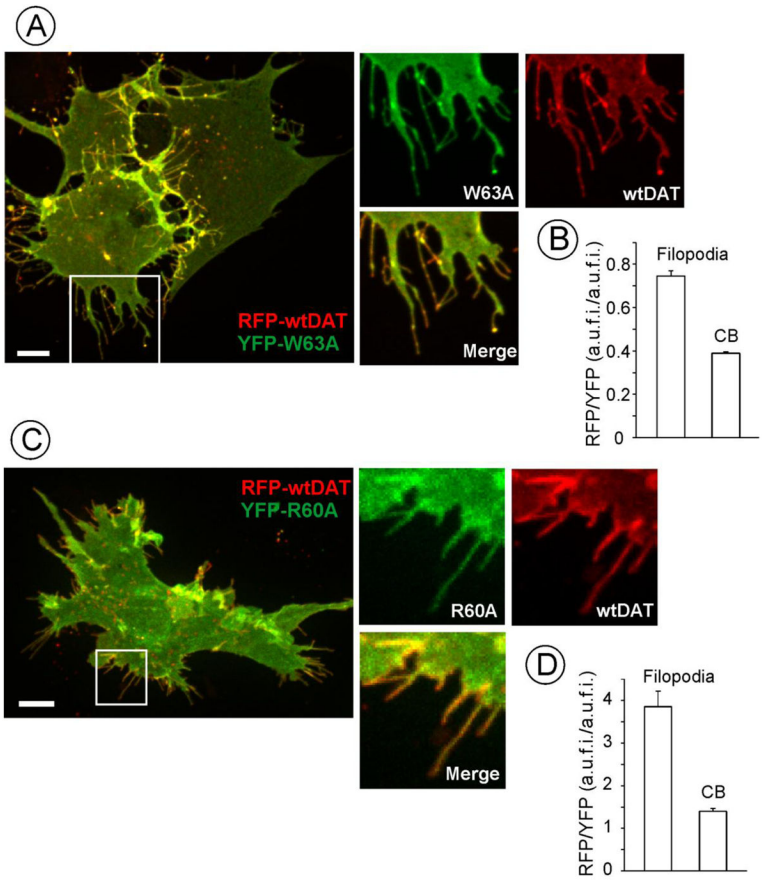

Figure 3. DAT mutants are not enriched in filopodia

RFP-HA-DAT was transiently co-expressed with W63A (**A**, **B**) or R60A (**C**, **D**) YFP-HA-DAT mutants in PAE cells, and cells were imaged through 561 (RFP) and 515 (YFP) filter channels. Maximal projection images of 3D images are presented in (**A)** and (**C)**. Insets show high magnification of the region marked by the white rectangle to demonstrate the enrichment of RFP-HA-DAT in distal filopodia regions as compared to DAT mutants. Scale bars, 10 μm.

(**B) and (D)**, Quantification of RFP/YFP fluorescence ratios in filopodia and other parts of the cells (“cell body”, ***CB***) in images presented in ***A*** and ***C***. Graph bars represent mean values (+S.E.M.) of the RFP/YFP ratios from 30–35 filopodia or ROIs within CB. *A.u.f.i.*, arbitrary units of fluorescence intensity.

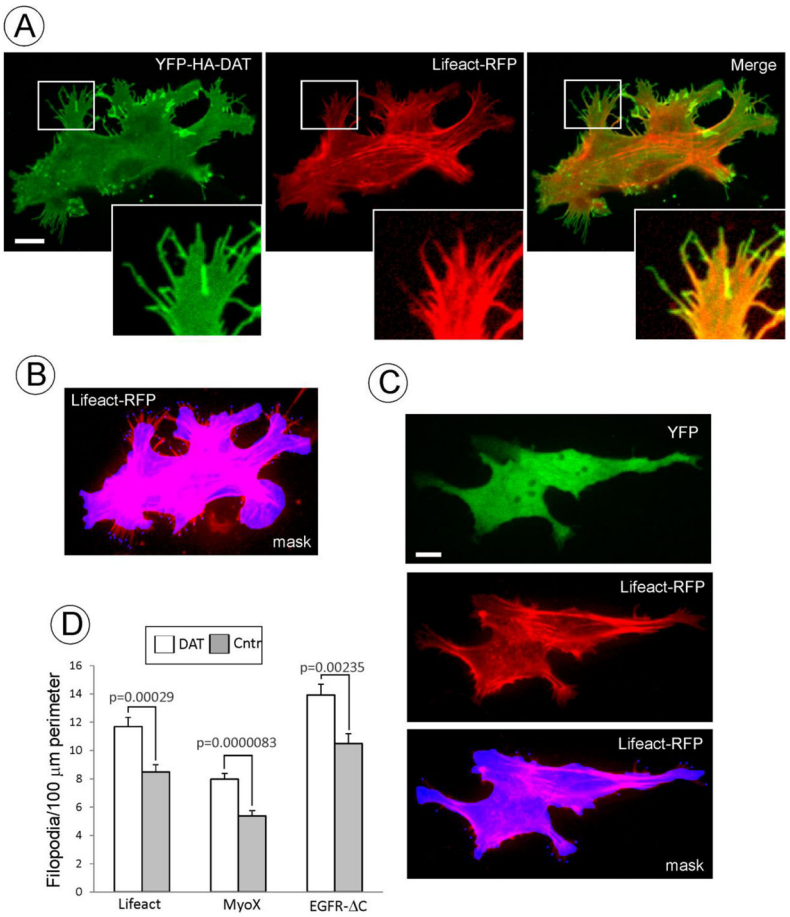

Figure 4. DAT induces filopodia formation

(A) YFP-HA-DAT and Lifeact-RFP were transiently expressed in PAE cells. Z-stack of 10 confocal images (400 nm stepsize) of living cells was acquired through 515 (YFP) and 651 (RFP) channels at 37°C. RFP image is presented with the gamma for the 561 channel set to 0.5 to allow for better visualization of the low-intensity Lifeact-RFP signals in filopodia without interference of the bright signal of the cell cortex. Insets show high magnification of the region marked by the white rectangle to demonstrate enrichment of YFP-HA-DAT in distal filopodia regions compared to Lifeact-RFP.

(B) Example of the selection mask used for counting peripheral filopodia. Mask was manually generated by encircling the perimeter of the cell Lifeact-RFP fluorescence. Filopodia extending for more than 2 µm outside of the mask were marked. Perimeter of the cell body was calculated, and the number of filopodia was counted using the SlideBook statistics module. In the example presented, there are 11.6 filopodia per 100 µm of cell perimeter.

(C) YFP and Lifeact-RFP were transiently expressed in PAE cells. Image acquisition and presentation are identical to (A) and (B). In the example of the selection mask used for counting peripheral filopodia (as described in B), there are 4.5 filopodia per 100 µm of cell perimeter.

(**D**) Quantifications of the filopodia density (number per 100 µm of cell perimeter) were performed as described in ***B*** and ***C***. These calculations were carried out in living cells co-

expressing Lifeact-RFP with YFP (Cntr) or YFP-HA-DAT; PAE/YFP-HA-DAT and parental PAE cells (Cntr) by immunostaining (performed similar to Fig. 1A) and counting MyoX decorated filopodia; and in cells transiently co-expressing YFP-HA-DAT and EGFR-ΔC (see examples of images in Fig. 2A). Graph bars represent mean values (+/−S.E.M.) of filopodia number per cell perimeter from 30–40 cells in each experimental variant. Scale bars, 10 μm.

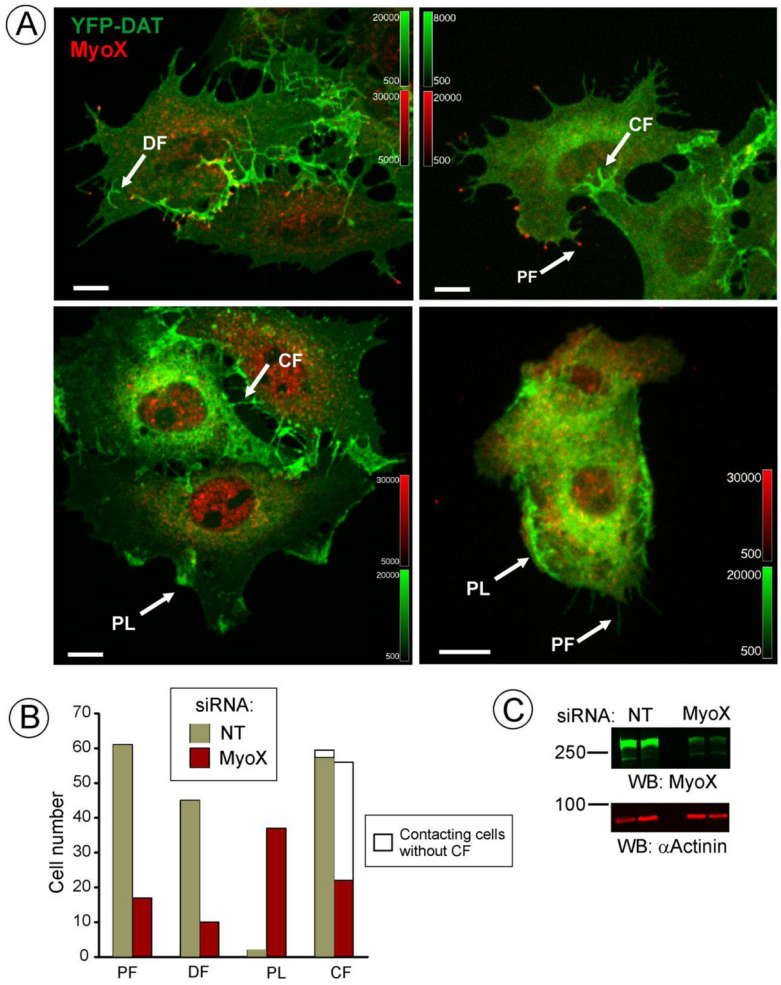

Figure 5. Effect of MyoX knockdown on DAT-containing filopodia

(A) PAE/YFP-HA-DAT cells were transfected with non-targeting (NT) or MyoX siRNAs and used for experiments 3–4 days later. The cells were fixed and immunostained with MyoX antibodies (dilution 1:500) followed by secondary antibody conjugated to Cy3. 3D images were acquired through 561 (red, MyoX) and 515 (green, YFP) channels. Two examples of control and MyoX-depleted cells are shown. Maximal projection of the z-stack is presented. Examples of peripheral (***PF***), dorsal filopodia (***DF***), filopodia connecting two cells (***CF***) and peripheral lamellopodia-like structures (PL) that were scored in individual cells for calculations presented in (**B**) are indicated by arrows. Scale bars, 10 μm.

(B) Calculations from two experiments in PAE/YFP-HA-DAT and PAE/RFP-HA-DAT cells performed similar to the experiment presented in (***A***). Total 3-D images of 65 NT- and 65 MyoX-siRNA transfected cells were analyzed in a blind fashion. The results are presented as numbers of cells that manifest DAT-rich peripheral filopodia (***PF***) (>5 PF per cell), dorsal filopodia (***DF***) (>2 DF per cell), peripheral lamellopodia-like structures (***PL***) (>1 PL per cell), cell-cell connecting filopodia (***CF***) (>3 per cell) and cells contacting other cells but not having CFs, all exemplified in (***A***).

C, Western blot detection of MyoX and α-actinin (loading control) in cells transfected with NT or MyoX siRNA. Duplicates are presented. The averaged knock-down efficiency in multiple experiments was 85.5% +/−6.2% (S.D.).

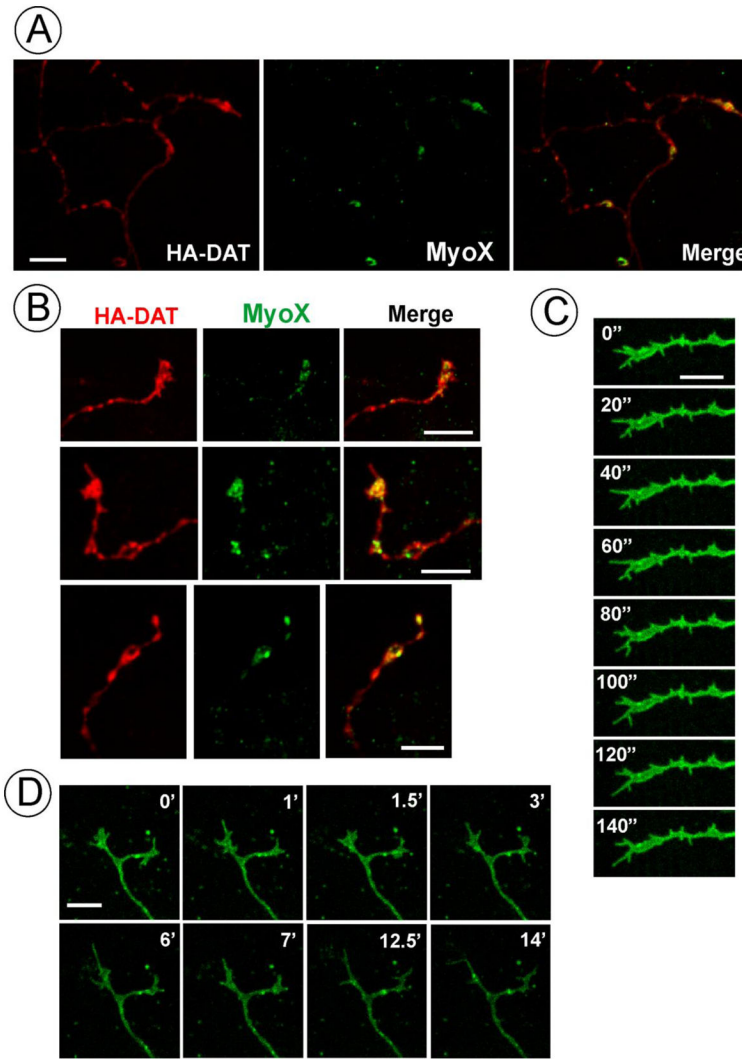

Figure 6. Localization of MyoX in dopaminergic neurons

(A) and (B), Primary midbrain neuronal cultures from HA-DAT mice were fixed and stained with HA (2 μg/ml) and MyoX (1:100) antibodies followed by corresponding secondary antibodies. 3-D imaging was performed as in Fig. 1. Several examples of MyoX localization in growth cones and axonal varicosities are presented.

(C) and (D), Primary midbrain neuronal cultures were incubated with HA11 conjugated wisth Alexa488 (10 μg/ml) for 2 hrs at 37°C, washed and 4-D (3D and time-lapse) live-cell imaging was performed at 37°C. Individual selected time frames are shown to demonstrate high motility of filopodia in growth cones. Times are in seconds (***C***) or minutes (***D***). See Supplemental videos S2 (***C***) and S3 (***D***).

Scale bars, 10 μm.